The Company of **Biologists**

RESEARCH ARTICLE

Comparison of human gastrocnemius forces predicted by Hill-type muscle models and estimated from ultrasound images

Taylor J. M. Dick[1],[*], Andrew A. Biewener[2] and James M. Wakeling[1]

ABSTRACT

Hill-type models are ubiquitous in the field of biomechanics, providing estimates of a muscle's force as a function of its activation state and its assumed force–length and force–velocity properties. However, despite their routine use, the accuracy with which Hill-type models predict the forces generated by muscles during submaximal, dynamic tasks remains largely unknown. This study compared human gastrocnemius forces predicted by Hill-type models with the forces estimated from ultrasound-based measures of tendon length changes and stiffness during cycling, over a range of loads and cadences. We tested both a traditional model, with one contractile element, and a differential model, with two contractile elements that accounted for independent contributions of slow and fast muscle fibres. Both models were driven by subject-specific, ultrasound-based measures of fascicle lengths, velocities and pennation angles and by activation patterns of slow and fast muscle fibres derived from surface electromyographic recordings. The models predicted, on average, 54% of the time-varying gastrocnemius forces estimated from the ultrasound-based methods. However, differences between predicted and estimated forces were smaller under low speed–high activation conditions, with models able to predict nearly 80% of the gastrocnemius force over a complete pedal cycle. Additionally, the predictions from the Hill-type muscle models tested here showed that a similar pattern of force production could be achieved for most conditions with and without accounting for the independent contributions of different muscle fibre types.

INTRODUCTION

Hill-type muscle models are ubiquitous in biomechanical analyses of human movement and more recently are being applied to animal studies to provide estimates of a muscle's force as a function of its activation state and assumed force–length and force–velocity properties. For example, Hill-type models have been used, together with reconstructions of musculoskeletal geometry, to analyse the moment-generating capacities of animals during terrestrial locomotion (O'Neill et al., 2013; Hutchinson et al., 2015) and to estimate the locomotor capabilities of extinct species based on fossil records (Hutchinson and Garcia, 2002). Muscle models have also been used in simulations of human locomotion to infer the functions of individual muscles during walking (Arnold et al., 2013) and running (Hamner et al., 2010) and to uncover important insights into the biomechanical factors that contribute to gait abnormalities (e.g. Peterson et al., 2010; Steele et al., 2010). However, the accuracy of the muscle forces predicted by Hill-type models, especially during submaximal, dynamic tasks, remains largely unknown.

The predictive accuracy of Hill-type models has been investigated in a small number of animal studies in which tendon forces were directly measured. For example, Sandercock and Heckman (1997) and Perreault et al. (2003) examined whether a Hill-type model could predict *in situ* forces generated by the cat soleus when they imposed length changes corresponding to those measured during locomotion. Their model reproduced soleus forces measured *in vivo*, using an implanted tendon buckle transducer, to within 10% of maximal tension during force rise (Sandercock and Heckman, 1997). However, at low motor unit firing rates, differences in the predicted and measured forces were greater than 50% (Perreault et al., 2003). Our own efforts to predict *in situ* and *in vivo* forces generated by the gastrocnemius muscles of goats (Wakeling et al., 2012; Lee et al., 2013) confirmed that Hill-type models are sensitive to assumptions about activation state and the force–velocity properties of the model's contractile element. For example, we have shown that Hill-type models reproduce the time-varying *in vivo* forces with an average r^2 of 0.40, and errors in force greater than 15% and 28% of maximum isometric force for the medial (MG) and lateral (LG) gastrocnemii of goats, respectively, when averaged across the gait cycle and different locomotor speeds. However, errors in force predictions were reduced when models incorporated the independent activations of slow and fast contractile elements, but only during the fastest locomotor speeds (Lee et al., 2013). Additionally, Millard and co-workers (2013) have demonstrated that Hill-type models are better able to reproduce muscle forces under maximally activated conditions in comparison to submaximally activated conditions. They compared the ability of three different Hill-type formulations to reproduce *in vivo* forces measured in the cat soleus under maximally active (Krylow and Sandercock, 1997) and submaximally active conditions (Perreault et al., 2003) and found that average errors were 12% of maximum tension for maximal contractions but increased to more than 17% for submaximal contractions. Together, these previous studies and others leave many unanswered questions in regards to the ability of Hill-type models to reproduce time-varying muscle force.

To gain more insight into the strengths and weaknesses of Hill-type models, independent estimates of time-varying muscle forces, for a wide range of movements, are needed. However, muscle forces often cannot be directly measured. We have recently developed an ultrasound-based approach to indirectly estimate the *in vivo* forces generated by the human triceps surae muscles during dynamic tasks (Dick et al., 2016). In particular, the gastrocnemius–Achilles tendon (AT) complex is advantageous because of its superficial location and short fascicles, which allow us to use ultrasound to measure

[1]Department of Biomedical Physiology and Kinesiology, Simon Fraser University, Burnaby, BC, Canada V5A 1S6. [2]Concord Field Station, Harvard University, Bedford, MA 01730, USA.

*Author for correspondence (taylor_dick@sfu.ca)

T.J.M.D., 0000-0001-8371-6247

both tendon and fascicle length changes during movement, and couple these measurements with subject-specific estimates of tendon stiffness and slack lengths to estimate time-varying forces. This is the first study to test Hill-type models against *in vivo* estimates of time-varying muscle forces from human subjects at a range of mechanical conditions.

Electromyographic (EMG) recordings from the gastrocnemii of cyclists have shown that the activation patterns of different muscle fibre types vary with cadence (Citterio and Agostoni, 1984; Wakeling et al., 2006; Wakeling and Horn, 2009). However, while muscles are composed of a mix of slow and fast fibres with different physiological and biomechanical properties, Hill-type models are typically composed of a single contractile element with force–length and force–velocity properties that have been estimated from *in vitro* data collected from single fibres under maximally activated conditions. To represent whole muscle, the fibre's force is scaled based on the muscle's level of activation, accounting for the muscle's physiological cross-sectional area, fibre length, pennation angle and parallel elasticity. Here, we tested a traditional Hill-type model, with one contractile element, compared with a differential model, having independent slow and fast contractile elements to account for the contributions of slow and fast muscle fibres. Both models were driven by subject-specific measures of fascicle length, velocity and pennation angle derived from ultrasound images and by activation patterns of slow and fast fibres derived from surface EMG recordings and wavelet-based time–frequency decomposition techniques (von Tscharner, 2000; Wakeling and Horn, 2009). We hypothesized that the two-element model would better reproduce the ultrasound-based estimates of gastrocnemius force at the higher cadences, where preferential recruitment of fast fibres has been reported (Citterio and Agostoni, 1984; Wakeling et al., 2006). This is an extension of our previous studies on the gastrocnemius muscles in goats, where we showed that a two-element model, driven by the independent activation of slow and fast muscle fibres, provided better predictions of time-varying muscle forces than traditional one-element models for some *in situ* (Wakeling et al., 2012) and *in vivo* (Lee et al., 2013) conditions.

MATERIALS AND METHODS

We collected comprehensive sets of kinematic, kinetic, EMG and ultrasound data from 16 competitive cyclists (8 male, 8 female; Table S1). Subjects pedalled on a stationary cycle ergometer (Indoor Trainer, SRM, Julich, Germany) at cadences between 60 and 140 rpm and crank loads between 14 and 44 N m. In this study, we analysed data from eight different combinations of cadence and load. We predicted the time-varying forces generated by each subject's LG and MG muscles during cycling using a one-element Hill-type model and a two-element Hill-type model (Fig. 1). The models were driven by fascicle lengths, velocities and pennation angles that we determined experimentally from ultrasound images, and by muscle activations calculated from simultaneous recordings of surface EMG (Fig. 1). We compared each subject's predicted LG and MG forces with the forces estimated *in vivo* from ultrasound-based measures of tendon length changes and stiffness (Fig. 1). Subjects gave informed consent and protocols were approved by the Institutional Ethics Review Boards at Simon Fraser University and Harvard University. The experimental protocol has been described and evaluated in a previous study (Dick et al., 2016), so a brief overview is provided here.

Muscle models for estimating LG and MG forces
We predicted the time-varying forces generated by each subject's LG and MG muscles during pedalling using a traditional Hill-type model:

$$F_m = F_{max}[\hat{a}(t)\hat{F}_a(\hat{l}_f)\hat{F}_a(\hat{v}) + \hat{F}_p(\hat{l}_f)]\cos\beta. \quad (1)$$

In previous efforts to predict gastrocnemius forces in goats, the intrinsic properties of the contractile element have been formulated in several different ways (Wakeling et al., 2012). However, it was found that the predicted forces were similar across the different formulations (Lee et al., 2013). In this study, we assigned contractile element properties that were consistent with a 'homogeneous one-element model' (Wakeling et al., 2012) that assumes the muscle consists of fibres with homogenous properties. In this model, the maximum intrinsic speed, often referred to as the maximum unloaded shortening velocity ($\hat{v}_0$), was the maximum intrinsic speed of the different fibre types weighted by their fractional cross-sectional areas. The curvature of the force–velocity relationship (α) was an intermediate value between the slow and fast fibres and was assumed to be the same for all the fibres within the muscle (Zajac, 1989; Wakeling et al., 2012; Lee et al., 2013) (Fig. 1C).

We also predicted the subjects' time-varying LG and MG forces using a 'differential two-element model' (Wakeling et al., 2012; Lee et al., 2013) that incorporates independently activated slow and fast contractile elements arranged in parallel (Fig. 1C):

$$F_m = F_{max}[[c_1\hat{a}(t)_{fast}\hat{F}_a(\hat{l}_f)\hat{F}_{a,fast}(\hat{v})$$
$$+ \hat{a}(t)_{slow}\hat{F}_a(\hat{l}_f)\hat{F}_{a,slow}(\hat{v})] + \hat{F}_p(\hat{l}_f)]\cos\beta. \quad (2)$$

In both models, total muscle force F_m is a function of the time-varying activation level $\hat{a}(t)$, the normalized active and passive force–length relationships $\hat{F}_a(\hat{l}_f)$ and $\hat{F}_p(\hat{l}_f)$, respectively, and the normalized force–velocity relationship $\hat{F}_a(\hat{v})$ (Fig. 1C). F_{max} represents the subject-specific maximum isometric force of either the LG or the MG:

$$F_{max} = \left(\frac{V_m}{l_{f,opt}}\right)\sigma_0. \quad (3)$$

F_{max} was calculated based on the muscle's scaled volume V_m estimated using the regression equations in Handsfield et al. (2014), and optimal fibre length $l_{f,opt}$ estimated from a subject-specific scaled musculoskeletal model (OpenSim v3.3; Delp et al., 2007; Arnold et al., 2010; Dick et al., 2016). σ_0 is estimated specific muscle stress (225 kPa; Spector et al., 1980; Roy et al., 1982) (Table S1). c_1 is a scaling factor that accounts for the lower power of the EMG signals that would be expected from action potentials with higher spectral frequencies (Wakeling et al., 2012). c_1 affects the balance between fast and slow fibre contributions and it was given a value of 2 as described below. F_{max} scales the fibre (or fascicle) force to whole-muscle force and pennation angle β allows the component of fascicle force that is aligned with the tendon to be estimated.

The normalized active force–length curve (Fig. 1C; Otten, 1987) was given by:

$$\hat{F}_a(l_f) = e^{-\left(\frac{\hat{l}_f^{0.6} - 1}{0.3}\right)^{2.3}}. \quad (4)$$

The normalized passive force–length curve (Fig. 1C) was given by:

$$\hat{F}_p = 2.64\hat{l}_f^2 - 5.30\hat{l}_f + 2.66 \quad \text{for} \quad \hat{l}_f > 1, \quad (5)$$

$$\hat{F}_p(\hat{l}_f) = 0 \quad \text{for} \quad \hat{l}_f \leq 1, \quad (6)$$
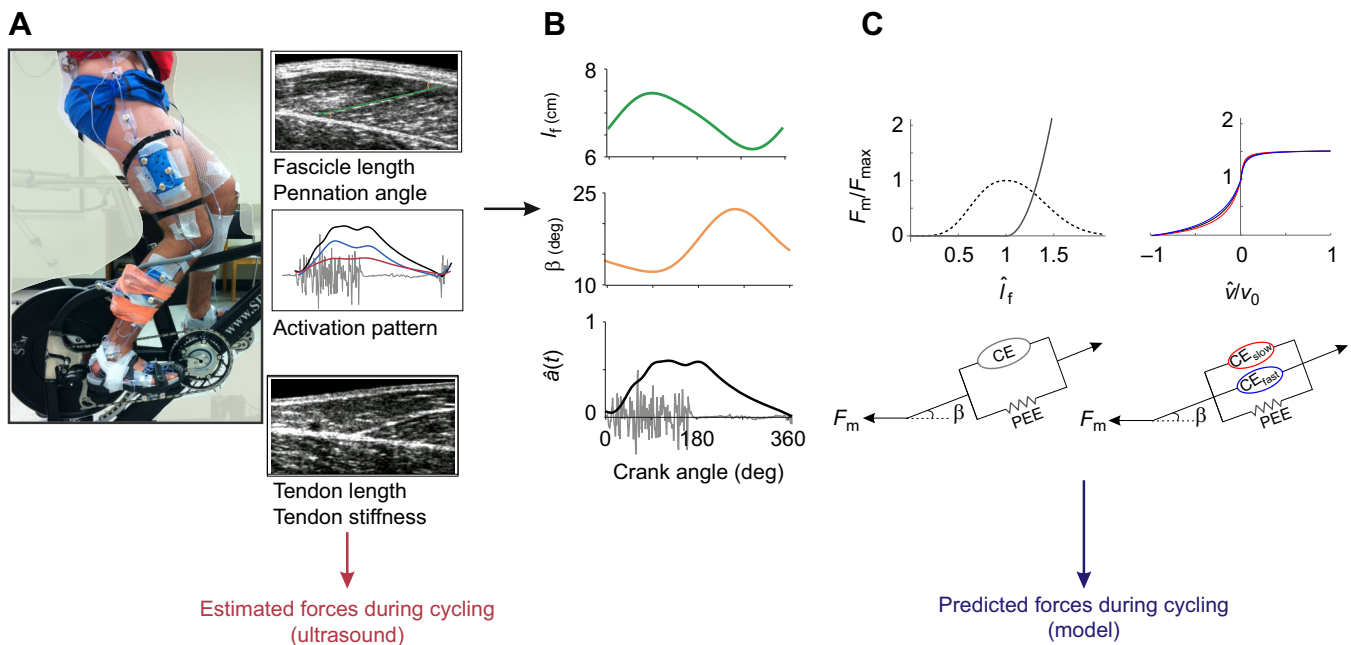
Fig. 1. Approach for comparing lateral gastrocnemius (LG) and medial gastrocnemius (MG) forces during cycling estimated from ultrasound-based measures of tendon length changes and stiffness and predicted from Hill-type muscle models. (A) During the cycling protocol, subjects pedalled on a stationary bike while we measured tendon lengths from tracked ultrasound images of the LG and MG muscle–tendon junctions, fascicle lengths and pennation angles from ultrasound images of the LG and MG muscle bellies, and activation patterns derived from surface electromyography. A trigger from the ultrasound system was used to synchronize all data. Forces were estimated from the tracked ultrasound images of tendon length changes during cycling and tendon stiffness measured for each subject in an isometric protocol (Dick et al., 2016). (B) The experimentally determined fascicle lengths l_f, pennation angles β and normalized muscle activations $\hat{a}(t)$ for total (black), slow (red) and fast (blue) motor units were used as inputs for the muscle models. (C) We tested a traditional one-element Hill-type muscle model and additionally a two-element model that accounted for the independent contributions of slow and fast muscles fibres. Estimated forces from the ultrasound-based approach were compared with the forces predicted from the models for the LG and MG. CE, contractile element; PEE, parallel elastic element; β, pennation angle. Refer to Table 1 for definitions of all symbols.

where $\hat{l}_f$ is fascicle length normalized to fascicle slack length $l_{0,f}$. $l_{0,f}$ was determined to be the length of the fascicle at tendon slack length. This passive force–length curve is similar to that provided by Millard and co-workers (2013) and is based on a combination of experimental data from chemically skinned human gastrocnemius fibres (Gollapudi and Lin, 2009) and rabbit whole muscles (Winters et al., 2011). The normalized force–velocity curve (Fig. 1C) was given by:

$$\hat{F}_a(\hat{v}) = \frac{1 + \left(\frac{\hat{v}}{\hat{v}_0}\right)}{1 - \left(\frac{\hat{v}}{\hat{v}_0 \alpha}\right)} \quad \text{for} \quad \hat{v} \le 0, \tag{7}$$

$$\hat{F}_a(\hat{v}) = 1.5 - 0.5 \frac{1 - \left(\frac{\hat{v}}{\hat{v}_0}\right)}{1 + \left(\frac{7.56\hat{v}}{\hat{v}_0 \alpha}\right)} \quad \text{for} \quad \hat{v} > 0, \tag{8}$$

where $\hat{v}$ is fascicle velocity normalized to $l_{0,f}$, which is equivalent to strain rate. α describes the curvature of the force–velocity relationship and depends on fibre type (Otten, 1987). A literature survey of 59 species from 88 papers concluded that the α values are 0.18 and 0.29 for slow and fast fibres, respectively (E. Hodson-Tole and J.M.W., unpublished observations). $\hat{v}_0$ is the maximum intrinsic speed, and we used values of 5 and 10 s^{-1} for the slow and fast fibres, respectively (Wakeling et al., 2012; Lee et al., 2013): 5 and 10 s^{-1} are thought to be within the appropriate range for human muscle (Faulkner et al., 1986; Epstein and Herzog, 1998) and are similar to values reported for mouse, cat and rat muscle measured at physiological temperatures, which range from 4.8 to 7.3 s^{-1} for slow fibres (Close, 1964; Spector et al., 1980; Askew and Marsh,

1998) and from 9.2 to 24.2 s^{-1} for fast fibres (Close, 1964, 1965; Luff, 1975; Spector et al., 1980). These values were also selected based on previous modelling results where the sensitivity of predicted forces to different values of $\hat{v}_0$ were assessed (Lee et al., 2013).

Histological analysis has shown that the human gastrocnemii contain equal cross-sectional areas of slow and fast muscle fibres (Johnson et al., 1973). Therefore, the one-element homogeneous model assumed that the active LG and MG have intrinsic properties that represent the average values for α and $\hat{v}_0$ between slow and fast fibres (α=0.235; $\hat{v}_0$=7.5 s^{-1}) (Wakeling et al., 2012; Lee et al., 2013).

The muscle models (Eqns 1 and 2) were driven directly by the experimentally derived activation, fascicle length and pennation angle, and the predicted muscle forces were subsequently compared with estimates of the tendon force. The models did not involve the balancing of the fascicle force with tendon force (series elastic element force), as is necessary if the whole muscle–tendon unit is incorporated in the model. As such, our approach (which parallels earlier animal studies: Hodson-Tole and Wakeling, 2009; Wakeling et al., 2012; Lee et al., 2013) circumvents the need to apply additional serial damping components to prevent high-frequency oscillations in the solution (Günther et al., 2007; Millard et al., 2013; Haeufle et al., 2014).

Experimental data for driving models
Subjects pedalled at eight different combinations of cadence and crank torque: 60 rpm at 44 N m, 80 rpm at 14 N m, 80 rpm at 26 N m, 80 rpm at 35 N m, 80 rpm at 44 N m, 100 rpm at 26 N m, 120 rpm at 13 N m and 140 rpm at 13 N m, corresponding to crank powers of 275, 115, 220, 290, 370, 270, 165 and 200 W, respectively. Each trial lasted 15 s. Each block of eight

Table 1. Model and equation parameters

Parameter	Definition	Source
$\hat{a}(t)$	Normalized activation	Derived from measured EMG (see Eqn 10)
c_1	Scaling factor, represents the lower EMG excitations that would be expected from action potentials with higher spectral frequencies	Calculated, used a value of 2
$\hat{e}(t)$	Normalized excitation	Calculated from measured EMG
F_{LG}	Lateral gastrocnemius force	Calculated from tendon length, stiffness and slack length (see Eqn 1)
F_{MG}	Medial gastrocnemius force	Calculated from tendon length, stiffness and slack length (see Eqn 11)
$\hat{F}_a(l_f)$	Normalized active force–length relationship	Estimated from literature (Lee et al., 2013; see Eqn 4)
$\hat{F}_a(v)$	Normalized force–velocity relation	From the literature (see Eqns 7 and 8)
F_m	Muscle force	Calculated from model (Eqn 1)
F_{max}	Maximal isometric force	Estimated (see Eqn 3)
$\hat{F}_p(l_f)$	Normalized passive force–length relationship	Estimated from literature (Millard et al., 2013; Eqns 5 and 6)
$k_{SEE-LG,T}$	LG toe region tendon stiffness	Measured in Dick et al., 2016
$k_{SEE-MG,T}$	MG toe region tendon stiffness	Measured in Dick et al., 2016
k_{SEE-LG}	LG linear region tendon stiffness	Measured in Dick et al., 2016
k_{SEE-MG}	MG linear region tendon stiffness	Measured in Dick et al., 2016
l_{AT-LG}	LG tendon length	Measured using B-mode ultrasound
l_{AT-MG}	MG tendon length	Measured using B-mode ultrasound
$l_{0,AT-LG}$	LG tendon slack length	Estimated from l_{AT-LG} at 310 deg of pedal cycle
$l_{0,AT-MG}$	MG tendon slack length	Estimated from l_{AT-MG} at 310 deg of pedal cycle
l_f	Fascicle length	Measured using B-mode ultrasound
$l_{0,f}$	Fascicle slack length	Determined from l_f at $l_{0,AT}$
$\hat{v}$	Normalized fascicle velocity	Derived from l_f
$\hat{v}_0$	Maximum intrinsic speed	Estimated from literature (5 and 10 s^{-1} for slow and fast fibres)
V_m	Muscle volume	Estimated using the regression equations of Handsfield et al., 2014
α	Curvature of force–velocity relationship	Estimated from literature (0.18 and 0.29 for slow and fast muscle fibres; Wakeling et al., 2012; Lee et al., 2013)
β	Pennation angle	Measured using B-mode ultrasound
σ_0	Maximum isometric stress of muscle fibres	Estimated from literature (225 kPa; Spector et al., 1980; Roy et al., 1982)

experimental conditions was repeated, in a random order, four times so that we could separately image both the LG and MG muscle bellies and the LG and MG muscle–tendon junctions (MTJs). Subjects rested for 5 min in between blocks of conditions. 'Maximum effort' sprint trials (high power and cadence) were collected at the beginning and end of each session in an effort to elicit maximum muscle activity, and we used these data as a reference when normalizing muscle EMG intensity (e.g. Rouffet and Hautier, 2008). We used an optical motion capture system (Certus Optotrak, NDI, Waterloo, Canada) sampling at 100 Hz to track the 3D locations of 32 LED markers placed bilaterally on the lower extremities, the pedals and the ultrasound probe. Pedal reaction forces effective and ineffective (normal and radial) to the right and left cranks were recorded at 2000 Hz (Powerforce, Radlabor, Freiburg, Germany). Previously, we have verified that the plantarflexion moments estimated from ultrasound-based measures of tendon strain are consistent with the net ankle moments determined from inverse dynamics (Dick et al., 2016).

Muscle fascicle length and pennation angle

A linear-array B-mode ultrasound probe (7 MHz, 60 mm field-of-view; Echoblaster, Telemed, Vilnius, Lithuania) recording at 40 Hz was used to alternately image LG and MG fascicles from the right leg during pedalling. The order in which muscles were imaged was randomized; at the end of each block of conditions, the probe was re-positioned over the other muscle. The probe was secured in a custom-made foam support and positioned to image muscle fascicles that were in the middle of the muscle belly (Fig. S1), where the fascicle architecture is homogeneous (Maganaris et al., 1998), and in plane with the scanning image (Kawakami et al., 1993). An ultrasound gel pad (Parker Laboratories, NJ, USA) was placed at the probe–skin interface to enhance image quality and allow muscle bulging.

Ultrasound images were manually digitized (ImageJ, NIH, Bethesda, MD, USA) to determine each subject's time-varying

fascicle lengths and pennation angles for the eight pedalling conditions. Eight points in each ultrasound image were digitized – three points on each of the superficial and deep aponeuroses and two points on a representative muscle fascicle (Fig. S2). Pennation angle was calculated as the mean of the angles made by the fascicle with the deep and superficial aponeuroses. Fascicle lengths and pennation angles from 10 complete crank revolutions were fitted using a least-squares minimization of a Fourier series: $c_2+a_1\sin(\varnothing_1+\omega)+a_2\sin(\varnothing_2+2\omega)$, where c_2, a_1, a_2, $\varnothing_1$ and $\varnothing_2$ are fitted constants and ω is the crank angle. These fascicle lengths and pennation angles were used as inputs to the muscle models for each muscle, each pedalling condition and each subject.

Muscle activation patterns

Bipolar Ag/AgCl surface electrodes (10 mm diameter and 21 mm spacing; Norotrode; Myotronics, Kent, WA, USA) were used to record muscle excitations from the LG, MG, soleus and seven other muscles on the contralateral (left) limb to which the ultrasound transducer was placed. EMG signals were preamplified (gain 1000), band-pass filtered (bandwidth 10–500 Hz; Biovision, Wehrheim, Germany) and sampled at 2000 Hz as described elsewhere (e.g. Wakeling and Horn, 2009; Blake and Wakeling, 2014). Electrodes were placed in the mid-region of the muscle belly after the skin had been shaved and cleaned with isopropyl alcohol solution. We secured electrodes with stretchable adhesive bandages and tubular net bandages to reduce movement artefacts during pedalling.

Surface EMG signal has been shown to contain distinct frequency characteristics that allow for characterization of recruitment between different types of motor units (Wakeling and Rozitis, 2004; Reaz et al., 2006; Wakeling, 2009). We characterized EMG signals from the LG and MG in two different ways: first by total EMG intensity, representing all active motor units within the muscle, and second by the EMG intensity at the low- and high- frequency bands,

Table 2. Centre frequencies and scale factors of optimized wavelets

Muscle	$f_{c,low}$ (Hz)	s_{low}	$f_{c,high}$ (Hz)	s_{high}
LG	72.87	0.085	156.69	0.078
MG	62.32	0.078	146.95	0.051

Centre frequencies $f_{c,low}$ and $f_{c,high}$ and scale factors s_{low} and s_{high} that characterize the low- and high-frequency components from the EMG intensity spectra for the muscle-specific optimized wavelets (Eqn 9) for the lateral (LG) and medial (MG) gastrocnemii.

to represent the contributions of slow and fast motor units, respectively. EMG signals for the muscles were quantified by their intensities during each crank revolution. The total intensity is a close approximation to the power of the signal and was calculated across a 10–450 Hz frequency band using an EMG-specific wavelet analysis (von Tscharner, 2000). Optimized wavelets were derived, for each muscle, using principal component analysis to identify the major features of the intensity spectra from the 16 subjects (Wakeling and Rozitis, 2004; Von Tscharner and Goepfert, 2006; Hodson-Tole and Wakeling, 2007; Wakeling and Horn, 2009; Lee et al., 2011) (Fig. 2). A least-squares minimization of a wavelet function $\psi(f)$ (Eqn 9) was used to construct two optimized wavelets to describe the low- and high-frequency spectra that correspond to the slow and fast motor units:

$$\psi(f) = \left(\frac{f}{f_c}\right)^{f_c \cdot s} \cdot e^{\left(\frac{-f}{f_c}+1\right)f_c \cdot s}, \quad (9)$$

where s is a scaling factor that defines the width and shape of the wavelet and f_c is the centre frequency of the wavelet (von Tscharner, 2000) (Table 2).

To compare predicted forces derived from the total intensities (one-element model) with the forces derived from the optimized wavelets (two-element model), the time resolutions from the two approaches were defined to be the same; to do this, we set the Gauss filters at the end of the wavelet analysis to a 50 ms time resolution for all wavelets, which is within the range of physiological time to peak twitch for skeletal muscle (10 and 100 ms; Levin et al., 2000; Spägele et al., 1999). We used the square-root of the EMG intensity as a measure of muscle excitation e, as muscle force is linearly related to the EMG amplitude and not its power (Milner-Brown and Stein, 1975). A lower EMG intensity would be expected from action potentials with higher spectral frequencies (Wakeling et al., 2012). Here, we selected a value of $c_1=2$ (in Eqn 2) to scale the excitations (based on the ratio of their centre frequencies: Table 2) to account for this effect.

We used a first-order differential equation (transfer function) to estimate the active state of the muscle from the muscle excitation (Zajac, 1989) that is commonly used for modelling human muscle. This choice was partly motivated by a parallel project that will compare the muscle models from this study with muscle force

predictions from the OpenSim musculoskeletal simulation environment (Delp et al., 2007) that also uses this transfer function. However, it should be noted that other transfer functions are capable of estimating better activation dynamics (Hatze, 1977; Lee et al., 2011; Rockenfeller et al., 2015) but require more model parameters that are currently unknown for muscle in man:

$$\frac{d}{dt}(a) + \left[\frac{1}{\tau_{act}}(\beta_{act} + [1-\beta_{act}]e(t))\right]a(t) = \left(\frac{1}{\tau_{act}}\right)e(t). \quad (10)$$

The activation time constant τ_{act}, specific to slow and fast fibres, and the ratio β_{act} of the activation to deactivation time constants were derived using tetanic contraction data in the literature (Table 3). Histological analysis has shown that the human gastrocnemii contain equal cross-sectional areas of slow and fast muscle fibres (Johnson et al., 1973). Therefore, τ_{act} for the activation transfer function for the one-element model was calculated as the average between slow and fast fibres. The ratio of activation to deactivation, β_{act}, was independent of fibre-type as both activation and deactivation rates are associated with the motor-unit type (Burke et al., 1973). We used the transfer function to derive the active state for the whole muscle (from the total EMG intensity), as well as for slow and fast motor units. In order to make comparisons between the one- and two-element models, the activation level of the summed slow and fast motor units was scaled in amplitude to equal the total activation during the maximum-effort reference pedalling trials. Activation traces from 10 cycles were combined to compute a mean LG and MG total, slow and fast muscle activation trace for each pedalling condition. Activation levels for each muscle are presented as normalized values $\hat{a}(t)$ calculated relative to the maximum activation detected during the reference maximum-effort pedalling trials.

Experimental data for evaluating models
We estimated *in vivo* muscle forces from subject-specific tendon length changes and stiffness to evaluate the predictions of our Hill-type models. A linear-array B-mode ultrasound probe was secured over the LG or MG distal MTJ. A rigid-body cluster of LED markers (Prager et al., 1998) firmly attached to the ultrasound probe, allowed the 3D coordinates of the LG or MG MTJ to be tracked (ImageJ). We calculated the length changes of each tendon l_{AT-LG} or l_{AT-MG} during cycling as the distance from the AT insertion on the calcaneus (identified using an LED marker) to the 3D position of the LG or the MG MTJ. We estimated each muscle's contribution to tendon force, F_{LG} and F_{MG} (Eqn 11; shown for MG), during cycling based on the measured length changes l_{AT-LG} or l_{AT-MG}, the subject-specific values of toe region stiffness $k_{SEE-LG,T}$, $k_{SEE-MG,T}$ and linear region stiffness k_{SEE-LG}, k_{SEE-MG} for either the LG or MG (Table S1), and the tendon slack length $l_{0,AT-LG}$ or $l_{0,AT-MG}$:
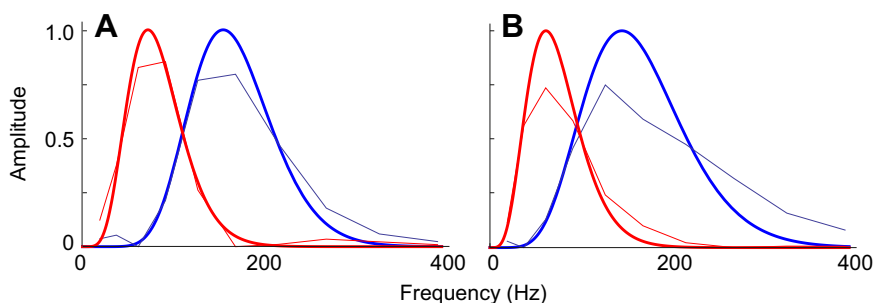

Fig. 2. Myoelectric intensity spectra reconstructed from the pooled frequency spectra (thin lines) and optimized wavelets (thick lines) for human LG (A) and MG (B). Low -frequency spectra are shown in red and high-frequency spectra in blue.

$$F_{MG} = \begin{cases} 0, & l_{AT-MG} \leq l_{0,AT-MG}, \\ k_{SEE-MG,T}(l_{AT-MG} - l_{0,AT-MG}), & l_{0,AT-MG} < l_{AT-MG} \leq (l_{0,AT-MG})1.0103, \\ k_{SEE-MG}(l_{AT-MG} - (l_{0,AT-MG})1.0103) + F_{max,T-MG}, & (l_{0,AT-MG})1.0103 < l_{AT-MG.} \end{cases} \qquad (11)$$

Tendon stiffness was estimated from ramped isometric tests (Morrison et al., 2015; Dick et al., 2016), where we quantified the total stiffness of the AT and also determined the proportion of the total AT stiffness contributed by the LG (k_{SEE-LG}) and MG (k_{SEE-MG}) separately. These muscle-specific stiffnesses were calculated based on the ratio of the maximum force-generating capacity F_{max} of either the LG or MG to the combined triceps surae maximum force (Table S1). Each tendon force–length curve had a toe region and a linear region. Linear stiffnesses, k_{SEE-LG} and k_{SEE-MG}, were subject specific but due to the difficulty in measuring the toe region properties of the force–length curve in all subjects during the isometric protocol (Dick et al., 2016), the same toe region stiffness, $k_{SEE-LG,T}$ and $k_{SEE-MG,T}$, was used for the LG and the MG in all subjects. $F_{max,T-MG}$ corresponds to the estimated force at the end of the toe region. Tendon slack lengths for the LG and MG portion of the AT ($l_{0,AT-LG}$ and $l_{0,AT-MG}$) were measured at 310 deg of the crank cycle, averaged over all cycles; this choice was motivated by published tendon buckle data (Gregor et al., 1987) showing force rise to occur after 310 deg. The time-varying tendon force from 10 cycles was used to compute a mean force trace for each condition.

Comparisons of predicted and estimated forces

We used the one- and two-element models to predict time-varying LG and MG forces for the 16 subjects and 8 pedalling conditions. Additionally, because the forces predicted by Hill-type models are sensitive to the assumed maximum intrinsic speed v_0 and curvature α of the force–velocity relationship (Shue et al., 1995; Perreault et al., 2003; Wakeling et al., 2012; Lee et al., 2013), we performed a sensitivity analysis and ran the models, varying the values of α (0.155–0.315) and v_0 (4–10 s^{-1}) to determine the extent to which the modelled forces were sensitive to these force–velocity properties. We compared the predicted forces with the forces estimated from ultrasound-based measures of tendon length changes and stiffness, and characterized differences across the crank cycle using two measures: the coefficient of determination r^2 and the root mean square error (RMSE). A general linear model ANOVA was conducted to determine whether differences in the r^2 and RMSE (dependent variable) existed between models, muscles, cycling conditions, subject (random), and values of α and v_0. We

Table 3. Constants for the excitation–activation transfer functions to determine muscle active state from EMG intensities

Constant	Fast excitation	Slow excitation	Total excitation
τ_{act} (ms)	25	45	35
β_{act}	0.6	0.6	0.6

τ_{act} is the activation time constant and β_{act} is the ratio of the activation to deactivation time.
To derive these constants, we manually traced (ImageJ) tetanic curves for cat slow and fast motor units (Kernell et al., 1983) and optimized the parameters τ_{act} and β_{act} to reproduce the force traces for a matched stimulation duration.

used a Chi-square test at each pedalling condition to determine whether the two-element model reproduced the estimated forces in the LG and MG better than the one-element model (higher r^2 and lower RMSE), over the entire crank cycle, more often than the one-element model. Additionally, an ANCOVA identified changes in the mean muscle activity for total, fast and slow motor units with cadence, crank load, and fascicle length $\hat{l}_f$ as covariates and subject as a random factor. $\hat{l}_f$ was included as a covariate because muscle strain has been shown to affect the frequency content of the EMG signal (Doud and Walsh, 1995). Differences were considered significant at the $P<0.05$ level. Data are reported as means±s.e.

RESULTS

The Hill-type models tested here, driven by EMG-derived activations and ultrasound-based measures of fascicle length, velocity and pennation angle, were able to capture the general features of the ultrasound-based estimates of force (Fig. 3). On average, the models performed with an r^2 of 0.54 and an RMSE of 13.52% F_{max} across muscles, conditions and models (Table 4; Fig. S3). However, models performed even better under low cadence–high load conditions, with r^2 values as high as 0.62 and 0.79 and errors as low as 8.98% F_{max} and 9.86% F_{max} for the LG and MG, respectively. A comparison of the modelled forces between the pedalling conditions, between muscles and between the one- and two-element models is shown in Table 4 and Fig. S3.

In both the LG and MG, there were minor differences between the muscle forces predicted by the two-element model when compared with the ultrasound-based estimates of tendon force and those
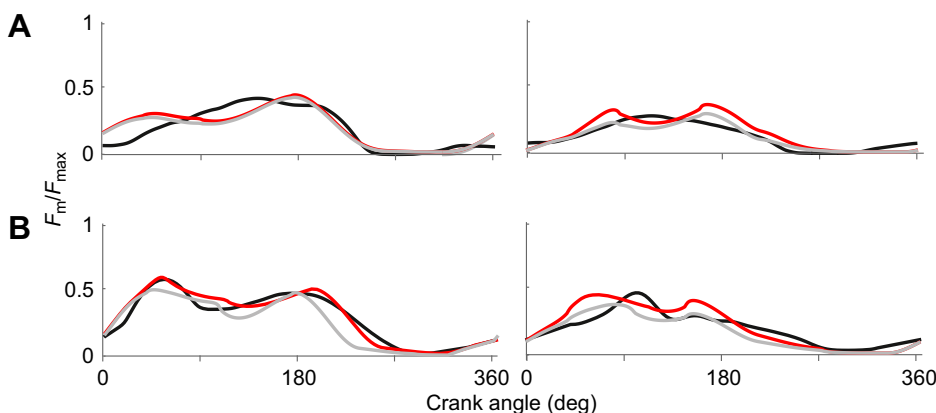
Fig. 3. Time-varying force profiles for the LG (left) and MG (right) with pedalling condition for one representative subject. (A) Pedalling at 60 rpm cadence at 44 N m crank torque. (B) Pedalling at 100 rpm at 26 N m. Ultrasound-based estimates of force are represented in black, and predicted forces from the one-element model in grey and from the two-element model in red. Muscle forces F_m are normalized to the maximum isometric force F_{max} of either the LG or the MG.

Table 4. Average LG and MG coefficient of determination r^2 and root mean square error RMSE between model predictions and ultrasound-based estimates of force, using the one-element and the two-element models across pedalling conditions

Cadence (rpm)	Crank load (N m)	LG				MG			
		r^2		RMSE (% F_{max})		r^2		RMSE (% F_{max})	
		One-element	Two-element	One-element	Two-element	One-element	Two-element	One-element	Two-element
60	44	0.54±0.07	0.52±0.07	8.98±0.86	9.38±0.95	0.79±0.03	0.78±0.03	10.17±1.60	9.86±1.26
80	14	0.46±0.07	0.47±0.07	10.98±0.83	11.32±1.05	0.64±0.05	0.65±0.05	10.60±0.99	10.77±0.89
80	26	0.61±0.03	0.62±0.04	10.27±1.47	10.45±1.40	0.66±0.05	0.66±0.05	10.83±1.20	10.67±1.04
80	35	0.46±0.07	0.46±0.07	10.88±1.20	11.46±1.09	0.68±0.05	0.68±0.05	11.96±1.49	11.36±1.40
80	44	0.55±0.08	0.55±0.08	13.05±2.33	13.78±1.95	0.71±0.05	0.71±0.05	12.39±1.86	12.09±1.59
100	26	0.41±0.08	0.42±0.09	15.47±2.44	14.90±2.36	0.50±0.07	0.51±0.07	18.25±2.03	18.26±1.82
120	13	0.38±0.08	0.40±0.09	16.49±1.99	15.78±1.73	0.45±0.05	0.48±0.05	16.93±2.09	17.45±2.01
140	13	0.29±0.06	0.32±0.05	21.91±3.50	21.22±3.36	0.46±0.08	0.49±0.08	17.53±2.25	17.43±2.25
	Average	0.46	0.47	13.50	13.51	0.61	0.63	13.65	13.48

Data are presented as means±s.e. (n=16); r^2 and RMSE were calculated for the time-varying forces across one complete pedal revolution.

predicted by the traditional one-element model. In particular, when averaged across subjects and conditions, the two-element model predicted forces with r^2 values of 0.47±0.09 and 0.63±0.1 for the LG and MG, respectively, compared with 0.46±0.1 and 0.61±0.12 for the one-element model LG and MG, respectively. RMSE errors were similar between the two models. The two-element model did perform significantly better than the one-element model at high cadences (100–140 rpm; Table S2), although the differences were small (Table 4; Fig. S3).

Consistent with previous literature (Wakeling et al., 2006; Blake and Wakeling, 2014), the conditions tested in our study elicited a range of activation patterns between slow and fast muscle fibres, providing the rationale to test the two-element model (Fig. 4). When averaged over the whole pedal cycle, the total activation increased with both crank load and cadence in both the LG and MG across all subjects ($P<0.05$). Activation of the slow motor units decreased with cadence (LG: P=0.02, MG: P=0.045) but increased with crank

load (LG and MG: $P<0.01$). Fast motor unit activation increased with both cadence and load in the LG and MG ($P<0.01$). Therefore, increased cadence resulted in a reduction of slow motor unit activity coupled with an increase in fast motor unit activity.

The Hill-type models tested in this study reproduced the estimated forces for the MG more accurately than for the LG. Both the one- and two-element models predicted forces with a higher r^2 over the crank cycle for the MG as compared with the LG across all pedalling conditions ($P<0.05$) (Table 4; Fig. S3). The average r^2 across subjects, conditions and models decreased from 0.62 (range: 0.45–0.79) for the MG to 0.47 (range: 0.29–0.62) for the LG. However, the average RMSE over the crank cycle was similar between muscles: 13.55% F_{max} (range: 9.86–18.25) for the MG and 13.51% F_{max} (range: 9.98–21.91) for the LG.

Time-varying patterns of the predicted and estimated forces, as assessed by r^2 and RMSE, showed greater differences at high cadences in comparison with low cadences (Table 4; Fig. S3); this
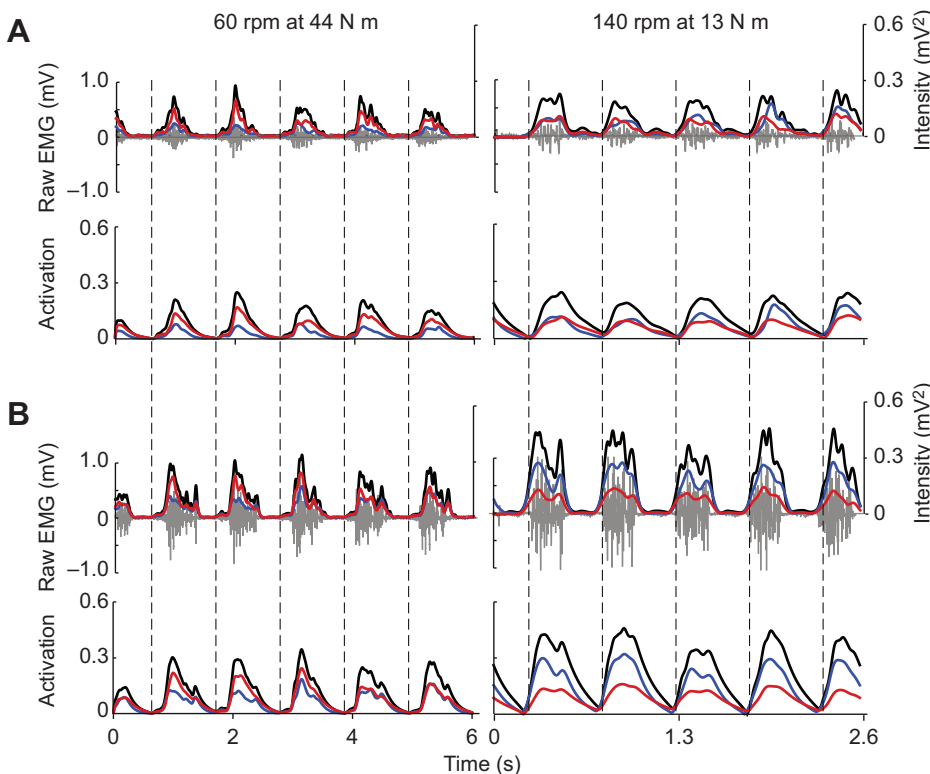

Fig. 4. Differential recruitment of slow and fast muscle fibres with pedalling condition for one representative subject. Raw EMG (grey) and total (black), slow (red) and fast (blue) intensity and activation traces for LG (A) and MG (B) when pedalling at 60 rpm at 44 N m (left panel) and 140 rpm at 13 N m (right panel). Vertical dashed lines show the timing of pedal top-dead-centre. These conditions have been chosen to highlight the differences in recruitment between slow and fast muscle fibres that can occur across the range of mechanical conditions tested here.

was a common feature for both the one-element and two-element models. In particular, when averaged across the two different models, the RMSE over the crank cycle was 11.1±1.2% F_{max} at cadences of 60–80 rpm and increased to 17.6±2.1% F_{max} at cadences of 100–140 rpm when averaged across muscles, subjects and conditions.

The forces predicted by the Hill-type models tested here were sensitive to the force–velocity curvature α used (Fig. 5). In both the LG and MG, the models predicted force with a higher r^2 and lower RMSE (data not shown) when using α=0.235 or α=0.315 for the one-element model, as compared to α=0.155 when averaged across all pedalling conditions (Fig. 5A). The most notable differences in model performance with α were evident at cadences of ≥100 rpm, where models predicted force with a higher r^2 and lower RMSE when using greater α values (Fig. 5A). In contrast, the predicted forces were not sensitive to the maximum intrinsic speed v_0 implemented within the models. These trends were similar for the one-element and two-element models tested (data shown for the one-element model; Fig. 5).

DISCUSSION
Our results reveal that Hill-type muscle models, driven by EMG-derived activation and ultrasound-based measurements of fascicle length, velocity and pennation angle, predicted, on average, 54% the gastrocnemius forces generated by human subjects during cycling, as estimated via ultrasound-based estimates of tendon length changes and stiffness. In general, the models performed best when the fascicles shortened at lower velocities and the activation levels were high, with models under these conditions able to predict nearly 80% of the medial gastrocnemius force over a complete pedal cycle. This work provides the first comparison of forces predicted by Hill-type models – driven with *in vivo* human experimental data under submaximal dynamic tasks – to ultrasound-based estimates of muscle–tendon force. The two-element model with independent slow and fast contractile elements showed no significant improvement for predicting time-varying and maximum muscle forces, when compared with a traditional one-element model for the slower conditions tested; however, small but significant improvements were noted at the fastest cadences. This suggests that other factors play an

important role in determining time-varying patterns and magnitudes of muscle force in addition to the contractile properties of the constituent motor units. Identifying the underlying sources of error in force predictions from Hill-type models remains challenging, particularly when having to rely on non-invasive estimates of muscle–tendon force. However, the approach described here provides an important step and an experimental framework for investigating how Hill-type models may be improved.

Differences between muscles and pedalling conditions
The performance of the Hill-type models depended on which muscle was being modelled. The human LG and MG vary in architecture (Maganaris et al., 1998), activation patterns (Wakeling et al., 2011) and motor-unit twitch profiles (Vandervoort and McComas, 1983). Specifically, the MG has shorter, more pennate fascicles than the LG (Wakeling et al., 2006; Ward et al., 2009), while the LG has a more complex architecture than the MG, with multiple heads that have different fascicle arrangements (Wolf et al., 1998). This complexity may have diminished our ability to accurately estimate representative fascicle lengths, velocities and pennation angles in the LG using ultrasound – and suggests that models are likely to be more accurate for muscles with homogeneous architecture. Consequently, these differences may help to explain the variation in model performance shown here, particularly the finding that models reproduced the estimated forces more closely across the pedal cycle for the MG than for the LG, which is consistent with the results from the gastrocnemii of goats (Lee et al., 2013).

The muscle models were compared with estimates of tendon force that were derived from ultrasound measures of tendon length and subject-specific tendon stiffness (methods described in Dick et al., 2016). The tendon stiffness for the LG and MG portions of the AT was previously determined on an isometric frame in which the knee was held at 130 deg and the subjects performed maximal effort plantarflexions (Morrison et al., 2015; Dick et al., 2016). However, it is possible that at different knee angles, where the relative lengths of the LG, MG and soleus are affected differently as a result of the biarticular nature of the LG and MG versus the uniarticular nature of the soleus, we may get a different value of stiffness and thus a
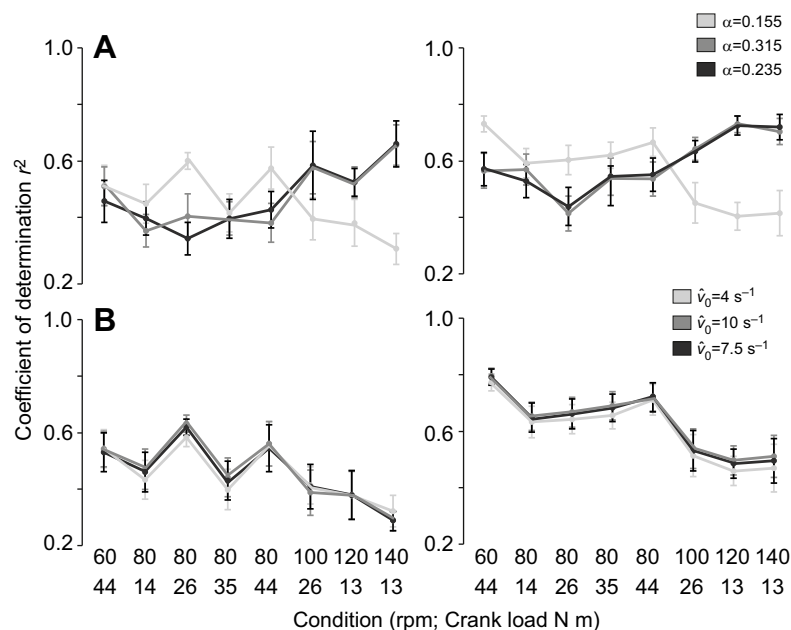

Fig. 5. Sensitivity of one-element model predictions to force-velocity parameters in the LG (left) and MG (right). (A) Curvature of force–velocity relationship, α. (B) Maximum intrinsic speed, $\hat{v}_0$. Data points represent the mean±s.e. across all subjects (*n*=16). Different values of α and $\hat{v}_0$ are shown using different shades of grey.

different value of force. During cycling, in the middle of the pedal upstroke (270 deg), the AT is unloaded and muscle activation is zero; consequently, both estimated tendon force and predicted muscle force will be zero. Towards the top of the pedal cycle, the AT starts to become loaded; however, as the knee is still relatively flexed, the contribution of the gastrocnemii to the combined AT force is likely to be less relative to the soleus than occurred during our isometric measures of force and tendon strain. This may lead to an over-estimation of the tendon force during this phase, although the forces predicted by the muscle models are independent of tendon stretch and are thus unaffected by this. However, when the knee angle reaches 130 deg at a crank angle of 90 deg, this matches the isometric test conditions and coincides with the period when the muscle forces are the greatest. Additionally, the ankle plantarflexors (LG, MG and soleus) have a similar activity during the low cadence–high load conditions (Dick et al., 2016), which most closely matches the isometric conditions for which tendon stiffness was determined. There was also a greater resolution of ultrasound frames per pedal cycle at the lowest cadences as a result of the finite sampling rate of the ultrasound scanner. Thus, we would expect the best match between the modelled muscle force and the estimated tendon stiffness to occur for the low cadence–high load conditions. Indeed, the r^2 reached 0.79 with a corresponding RMSE of 10% F_{max} for these conditions in the MG (Table 4), and this is likely to be the limit to the accuracy that can be achieved using these non-invasive experimental techniques.

The accuracy of the models tested here is partly limited by the measures of fascicle length, pennation angle and tendon length as well as estimates of fascicle and tendon slack length. We have previously shown that small increases in tendon slack length delayed the onset of AT force during cycling and decreased the magnitude of the predicted forces (Dick et al., 2016). Additionally, fascicle slack length is set at the time when the tendon is at its slack length. It is possible that the accuracy of these models could be further improved if the fascicle and tendon slack lengths were independently determined by optimization (e.g. Gerus et al., 2012; Gerus et al., 2015), rather than being experimentally guided; however, this was not the purpose of this study. Additionally, the overall accuracy of the muscle model is scaled by F_{max} (Eqn 3), that was determined from both an optimal fibre length and an estimated muscle volume that were derived from regression equations from other studies (Delp et al., 2007; Handsfield et al., 2014).

Comparison with Hill-type models in the literature
Previous studies have assessed the accuracy of Hill-type models against direct measures of force from tendon buckle recordings in animals (Sandercock and Heckman, 1997; Perreault et al., 2003; Wakeling et al., 2012; Lee et al., 2013; Millard et al., 2013; Kim et al., 2015) or against measures of heat and work (Umberger et al., 2003; Lichtwark and Wilson, 2005). In particular, modelling *in situ* forces yielded higher r^2 values (Sandercock and Heckman, 1997; Perreault et al., 2003; Wakeling et al., 2012) than *in vivo* forces (Lee et al., 2013), which probably relates to the more controlled contractions studied during *in situ* experiments in comparison to *in vivo* experiments. The errors achieved in this study for the slower cadences (RMSE of 10% F_{max} with r^2 of 0.79) match the best *in vivo* models (RMSE of 10%; Lee et al., 2013) that have been achieved in animal studies where the data were collected from more invasive techniques (fine-wire EMG for activation, sonomicrometry for fascicle length, and tendon buckles for force).

Differences between the forces predicted by the one- and two-element models in this study were smaller than the differences predicted by similar one- and two-element models in the goat gastrocnemius (Lee et al., 2013). However, both the goat study and the current study did find the only significant improvements in the two-element model to occur at the fastest muscle strain rates. Surprisingly, the greater benefits from the two-element model occurred in the goat study, which did not show such fast strains rates as seen here. However, the differences in model performance may reflect the additional challenges of extracting EMG information from surface EMG signals in humans, or from the effect whereby contractile differences between muscle fibre types may be mitigated in larger muscles that are submaximally activated (Holt et al., 2014; Ross and Wakeling, 2016).

Intrinsic properties and the two-element model
Previous studies have shown that the errors in forces predicted by Hill-type models are often related to the assumed maximum intrinsic speed v_0 and curvature α of the force–velocity relationship (Shue et al., 1995; Perreault et al., 2003; Wakeling et al., 2012; Lee et al., 2013). In contrast to our previous study (Lee et al., 2013), predicted forces of the models here were not sensitive to maximum intrinsic speed v_0 (Fig. 5). However, predicted forces were sensitive, in a cadence-specific manner, to the curvature α of the force–velocity relationship. Most notably, models reproduced the estimated forces more closely (higher r^2 and lower RMSE over the pedal cycle) using low α values at low cadences, but models performed better using higher α values at high cadences (Fig. 5A). For a given shortening velocity, a higher α would result in a larger force. As mentioned previously, slow fibres are characterized by a higher curvature (lower α) whereas fast fibres are characterized by a lower curvature (higher α) (Otten, 1987; Umberger et al., 2003). These results suggest that the forces predicted by traditional Hill-type models may be improved by incorporating a force–velocity curvature α that varies appropriately with the type of muscle fibres recruited for the specific mechanical demands of the task – a larger α for high-speed tasks where faster fibres are recruited, and a smaller α for low-speed tasks where slower fibres are recruited. Umberger and colleagues (2003) have previously alluded to this, and have shown that Hill-type models with force–velocity parameters, to include v_0 and α, that are matched to the proportions of slow and fast muscle fibres, generate reasonable predictions of whole-muscle energetics during isolated muscle contractions, single joint motion and whole-body movement.

Consistent with previous cycling studies (Wakeling et al., 2006; Wakeling and Horn, 2009; Blake and Wakeling, 2014), higher cadences elicited differential recruitment patterns that displayed an increase in the activation of the faster motor units coupled with a decrease in the activation of the slower motor units (Fig. 4). However, the differences between predicted forces for the one- and two-element models at even these highest cadences were minor (average 3%). This could be attributed to the fact that (i) the one-element model was not sensitive to $\hat{v}_0$, (ii) the differences in recruitment across the range of loads and cadences tested here may not have been large enough to elicit substantial differences in model performance, or (iii) the forces from human-sized muscle at submaximal activation may be less sensitive to differences in fibre-type recruitment than previously expected. To date, our understanding of whole-muscle behaviour has largely come from studies in which muscles are maximally activated, and from single-fibre data or data from smaller muscles (<10 g). However, recent evidence suggests that muscle behaviour also depends on the

muscle's size (Ross and Wakeling, 2016) and level of activation (Rack and Westbury, 1969; Josephson and Edman, 1988; Rassier et al., 1999; Holt and Azizi, 2014, 2016; Holt et al., 2014; Ross and Wakeling, 2016). Understanding the role of different fibre types within large mixed muscles during voluntary submaximal contractions is clearly an avenue that warrants further investigation.

Conclusions

In this study, we compared gastrocnemius forces predicted by Hill-type models with the forces estimated from ultrasound-based measures of tendon length change and stiffness. Similar forces were predicted for the traditional one-element model and the two-element model that accounted for the independent contributions of different muscle fibre types across most of the speeds tested, and the models performed best when fascicle velocities were low and muscle activation was high. What additional factors should we consider in order to yield more accurate muscle models? Future work should aim to additionally consider the mechanical effects of a muscle's physical properties (e.g. mass, viscosity), as well as the potential contributions of elastic tissue (e.g. aponeurosis) and surrounding structures on muscle contractile function. This is likely to be critical for improving the reliability of muscle models as well as for understanding the mechanisms underlying whole-muscle function during dynamic sub-maximal contractions – which we currently know little about. Benchmark experimental data sets, like the data we have analysed here, are necessary and useful for testing and improving models.

Author contributions
T.J.M.D., A.A.B and J.M.W. designed the experiments. T.J.M.D. and J.M.W. conducted the experiments. T.J.M.D. analysed the data and wrote the first draft of the manuscript. J.M.W. and A.A.B. provided guidance throughout the study, assisted with writing and approved the manuscript.

Supplementary information
Supplementary information available online at
http://jeb.biologists.org/lookup/doi/10.1242/jeb.154807.supplemental

References
Arnold, E. M., Ward, S. R., Lieber, R. L. and Delp, S. L. (2010). A model of the lower limb for analysis of human movement. *Ann. Biomed. Eng.* **38**, 269-279.
Arnold, E. M., Hamner, S. R., Seth, A., Millard, M. and Delp, S. L. (2013). How muscle fiber lengths and velocities affect muscle force generation as humans walk and run at different speeds. *J. Exp. Biol.* **216**, 2150-2160.
Askew, G. N. and Marsh, R. L. (1998). Optimal shortening velocity (V/Vmax) of skeletal muscle during cyclical contractions: length-force effects and velocity-dependent activation and deactivation. *J. Exp. Biol.* **201**, 1527-1540.
Blake, O. M. and Wakeling, J. M. (2014). Early deactivation of slower muscle fibres at high movement frequencies. *J. Exp. Biol.* **217**, 3528-3534.
Burke, R. E., Levine, D. N., Tsairis, P. and Zajac, F. E. (1973). Physiological types and histochemical profiles in motor units of the cat gastrocnemius. *J. Physiol.* **234**, 723-748.
Citterio, G. and Agostoni, E. (1984). Selective activation of quadriceps muscle fibers according to bicycling rate. *J. Appl. Physiol.* **57**, 371-379.
Close, R. I. (1964). Dynamic properties of fast and slow skeletal muscles of the rat during development. *J. Physiol.* **173**, 74-95.
Close, R. I. (1965). Force: velocity properties of mouse muscles. *Nature* **206**, 718-719.
Delp, S. L., Anderson, F. C., Arnold, A. S., Loan, P., Habib, A., John, C. T., Guendelman, E. and Thelen, D. G. (2007). OpenSim: open-source software to create and analyze dynamic simulations of movement. *IEEE Trans. Biomed. Eng.* **54**, 1940-1950.
Dick, T. J. M., Arnold, A. S. and Wakeling, J. M. (2016). Quantifying Achilles tendon force *in vivo* from ultrasound images. *J. Biomech.* **49**, 3200-3320.
Doud, J. R. and Walsh, J. M. (1995). Muscle fatigue and muscle length interaction: effect on the EMG frequency components. *Electromyogr. Clin. Neurophysiol.* **35**, 331-339.
Epstein, M. and Herzog, W. (1998). *Theoretical Models of Skeletal Muscles: Biological and Mathematical Considerations*. New York: John Wiley and Sons.
Faulkner, J. A., Claflin, D. R. and McCully, K. K. (1986). Power output of fast and slow fibers from human skeletal muscles. In *Human Muscle Power* (ed. N. L. Jones, N. McCartney and A. J. McComas), pp. 81-94. Champaign, IL: Human Kinetics.
Gerus, P., Rao, G. and Berton, E. (2012). Subject-specific tendon-aponeurosis definition in Hill-type model predicts higher muscle forces in dynamic tasks. *PLoS ONE* **7**, e44406.
Gerus, P., Rao, G. and Berton, E. (2015). Ultrasound-based subject-specific parameters improve fascicle behaviour estimation in Hill-type muscle model. *Comput. Methods Biomech. Biomed. Engin.* **18**, 116-123.
Gollapudi, S. K. and Lin, D. C. (2009). Experimental determination of sarcomere force–length relationship in type-I human skeletal muscle fibers. *J. Biomech.* **42**, 2011-2016.
Gregor, R. J., Komi, P. V. and Järvinen, M. (1987). Achilles tendon forces during cycling. *Int. J. Sports. Med.* **8**, S9-S14.
Günther, M., Schmitt, S. and Wank, V. (2007). High-frequency oscillations as a consequence of neglected serial damping in Hill-type muscle models. *Biol. Cybern.* **97**, 63-79.
Haeufle, D. F. B., Günther, M., Bayer, A. and Schmitt, S. (2014). Hill-type muscle model with serial damping and eccentric force-velocity relation. *J. Biomech.* **47**, 1531-1536.
Hamner, S. R., Seth, A. and Delp, S. L. (2010). Muscle contributions to propulsion and support during running. *J. Biomech.* **43**, 2709-2716.
Handsfield, G. G., Meyer, C. H., Hart, J. M., Abel, M. F. and Blemker, S. S. (2014). Relationships of 35 lower limb muscles to height and body mass quantified using MRI. *J. Biomech.* **47**, 631-638.
Hatze, H. (1977). A myocybernetic control model of skeletal muscle. *Biol. Cybern.* **25**, 103-119.
Hodson-Tole, E. F. and Wakeling, J. M. (2007). Variations in motor unit recruitment patterns occur within and between muscles in the running rat (Rattus norvegicus). *J. Exp. Biol.* **210**, 2333-2345.
Hodson-Tole, E. F. and Wakeling, J. M. (2009). Motor unit recruitment for dynamic tasks: current understanding and future directions. *J. Comp. Physiol. B* **179**, 57-66.
Holt, N. C. and Azizi, E. (2014). What drives activation-dependent shifts in the force–length curve? *Biol. Lett.* **10**, 20140651.
Holt, N. C. and Azizi, E. (2016). The effect of activation level on muscle function during locomotion: are optimal lengths and velocities always used? *Proc. R. Soc. B Biol. Sci.* **283**, 20152832.
Holt, N. C., Wakeling, J. M. and Biewener, A. A. (2014). The effect of fast and slow motor unit activation on whole-muscle mechanical performance: the size principle may not pose a mechanical paradox. *Proc. R. Soc. B Biol. Sci.* **281**, 20140002.
Hutchinson, J. R. and Garcia, M. (2002). Tyrannosaurus was not a fast runner. *Nature* **415**, 1018-1021.
Hutchinson, J. R., Rankin, J. W., Rubenson, J., Rosenbluth, K. H., Siston, R. A. and Delp, S. L. (2015). Musculoskeletal modelling of an ostrich (Struthio camelus) pelvic limb: influence of limb orientation on muscular capacity during locomotion. *PeerJ* **3**, e1001.
Johnson, M. A., Polgar, J., Weightman, D. and Appleton, D. (1973). Data on the distribution of fibre types in thirty-six human muscles. An autopsy study. *J. Neurol. Sci.* **18**, 111-129.
Josephson, R. K. and Edman, K. A. P. (1988). The consequences of fibre heterogeneity on the force-velocity relation of skeletal muscle. *Acta Physiol. Scand.* **132**, 341-352.
Kawakami, Y., Abe, T. and Fukunaga, T. (1993). Muscle-fiber pennation angles are greater in hypertrophied than in normal muscles. *J. Appl. Physiol.* **74**, 2740-2744.
Kernell, D., Eerbeek, O. and Verhey, B. A. (1983). Relation between isometric force and stimulus rate in cat's hindlimb motor units of different twitch contraction time. *Exp. Brain Res.* **50**, 220-227.
Kim, H., Sandercock, T. G. and Heckman, C. J. (2015). An action potential-driven model of soleus muscle activation dynamics for locomotor-like movements. *J. Neural Eng.* **12**, 046025.
Krylow, A. M. and Sandercock, T. G. (1997). Dynamic force responses of muscle involving eccentric contraction. *J. Biomech.* **30**, 27-33.
Lee, S. S. M., de Boef Miara, M., Arnold-Rife, A. S., Biewener, A. A. and Wakeling, J. M. (2011). EMG analysis tuned for determining the timing and level of activation in different motor units. . *J. Electromyogr. Kinesiol.* **21**, 557-565.

Lee, S. S. M., Arnold, A. S., de Boef Miara, M., Biewener, A. A. and Wakeling, J. M. (2013). Accuracy of gastrocnemius muscles forces in walking and running goats predicted by one-element and two-element Hill-type models. *J. Biomech.* **46**, 2288-2295.

Levin, O., Mizrahi, J. and Isakov, E. (2000). Transcutaneous FES of the paralyzed quadriceps: is knee torque affected by unintended activation of the hamstrings. *J. Electromyogr. Kinesiol.* **10**, 47-58.

Lichtwark, G. A. and Wilson, A. M. (2005). A modified Hill muscle model that predicts muscle power output and efficiency during sinusoidal length changes. *J. Exp. Biol.* **208**, 2831-2843.

Luff, A. R. (1975). Dynamic properties of fast and slow skeletal muscles in the cat and rat following cross-reinnervation. *J. Physiol.* **248**, 83-96.

Maganaris, C. N., Baltzopoulos, V. and Sargeant, A. J. (1998). In vivo measurements of the triceps surae complex architecture in man: implications for muscle function. *J. Physiol.* **512**, 603-614.

Millard, M., Uchida, T., Seth, A. and Delp, S. L. (2013). Flexing computational muscle: modeling and simulation of musculotendon dynamics. *J. Biomed. Eng.* **135**, 021005.

Milner-Brown, H. S. and Stein, R. B. (1975). The relation between the surface electromyogram and muscular force. *J. Physiol.* **246**, 549-569.

Morrison, S. M., Dick, T. J. M. and Wakeling, J. M. (2015). Structural and mechanical properties of the human Achilles tendon: sex and strength effects. *J. Biomech.* **48**, 3530-3533.

O'Neill, M. C., Lee, L.-F., Larson, S. G., Demes, B., Stern, J. T. and Umberger, B. R. (2013). A three-dimensional musculoskeletal model of the chimpanzee (Pan troglodytes) pelvis and hind limb. *J. Exp. Biol.* **216**, 3709-3723.

Otten, E. (1987). A myocybernetic model of the jaw system of the rat. *J. Neurosci. Methods* **21**, 287-302.

Perreault, E. J., Heckman, C. J. and Sandercock, T. G. (2003). Hill muscle model errors during movement are greatest within the physiologically relevant range of motor unit firing rates. *J. Biomech.* **36**, 211-218.

Peterson, C. L., Hall, A. L., Kautz, S. A. and Neptune, R. R. (2010). Pre-swing deficits in forward propulsion, swing initiation and power generation by individual muscles during hemiparetic walking. *J. Biomech.* **43**, 2348-2355.

Prager, R. W., Rohling, R. N., Gee, A. H. and Berman, L. (1998). Rapid calibration for 3-D freehand ultrasound. *Ultrasound Med. Biol.* **24**, 855-869.

Rack, P. M. H. and Westbury, D. R. (1969). The effects of length and stimulus rate on tension in the isometric cat soleus muscle. *J. Physiol.* **204**, 443-460.

Rassier, D. E., MacIntosh, B. R. and Herzog, W. (1999). Length dependence of active force production in skeletal muscle. *J. Appl. Physiol.* **86**, 1445-1457.

Reaz, M. B. I., Hussain, M. S. and Mohd-Yasin, F. (2006). Techniques of EMG signal analysis: detection, processing, classification and applications. *Biol. Proced. Online* **8**, 11-35.

Rockenfeller, R., Günther, M., Schmitt, S. and Götz, T. (2015). Comparative sensitivity analysis of muscle activation dynamics. *Comput. Math. Methods Med.* **2015**, 585409.

Ross, S. A. and Wakeling, J. M. (2016). Muscle shortening velocity depends on tissue inertia and level of activation during submaximal contractions. *Biol. Lett.* **12**, 20151041.

Rouffet, D. M. and Hautier, C. A. (2008). EMG normalization to study muscle activation in cycling. *J. Electromyogr. Kinesiol.* **18**, 866-878.

Roy, R. R., Meadows, I. D., Baldwin, K. M. and Edgerton, V. R. (1982). Functional significance of compensatory overloaded rat fast muscle. *J. Appl. Physiol.* **52**, 473-478.

Sandercock, T. G. and Heckman, C. J. (1997). Force from cat soleus muscle during imposed locomotor-like movements: experimental data versus Hill-type model predictions. *J. Neurophysiol.* **77**, 1538-1552.

Shue, G., Crago, P. E. and Chizeck, H. J. (1995). Muscle-joint models incorporating activation dynamics, moment-angle, and moment-velocity properties. *IEEE Trans. Biomed. Eng.* **42**, 212-223.

Spägele, T., Kistner, A. and Gollhofer, A. (1999). Modelling, simulation and optimization of a human vertical jump. *J. Biomech.* **32**, 521-530.

Spector, S. A., Gardiner, P. F., Zernicke, R. F., Roy, R. R. and Edgerton, V. R. (1980). Muscle architecture and force-velocity characteristics of cat soleus and medial gastrocnemius: implications for motor control. *J. Neurophysiol.* **44**, 951-960.

Steele, K. M., Seth, A., Hicks, J. L., Schwartz, M. S. and Delp, S. L. (2010). Muscle contributions to support and progression during single-limb stance in crouch gait. *J. Biomech.* **43**, 2099-2105.

Umberger, B. R., Gerritsen, K. G. and Martin, P. E. (2003). A model of human muscle energy expenditure. *Comput. Methods Biomech. Biomed. Engin.* **6**, 99-111.

Vandervoort, A. A. and McComas, A. J. (1983). A comparison of the contractile properties of the human gastrocnemius and soleus muscles. *Eur. J. Appl. Physiol.* **51**, 435-440.

Von Tscharner, V. (2000). Intensity analysis in time-frequency space of surface myoelectric signals by wavelets of specified resolution. *J. Electromyogr. Kinesiol.* **10**, 433-445.

Von Tscharner, V. and Goepfert, B. (2006). Estimation of the interplay between groups of fast and slow muscle fibers of the tibialis anterior and gastrocnemius muscle while running. *J. Electromyogr. Kinesiol.* **16**, 188-197.

Wakeling, J. M. (2009). Patterns of motor recruitment can be determined using surface EMG. *J. Electromyogr. Kinesiol.* **19**, 199-207.

Wakeling, J. M. and Horn, T. (2009). Neuromechanics of muscle synergies during cycling. *J. Neurophysiol.* **101**, 843-854.

Wakeling, J. M. and Rozitis, A. I. (2004). Spectral properties of myoelectric signals from different motor units in the leg extensor muscles. *J. Exp. Biol.* **207**, 2519-2528.

Wakeling, J. M., Uehli, K. and Rozitis, A. I. (2006). Muscle fibre recruitment can respond to the mechanics of the muscle contraction. *Interface* **3**, 533-544.

Wakeling, J. M., Blake, O. M., Wong, I., Rana, M. and Lee, S. S. M. (2011). Movement mechanics as a determinate of muscle structure, recruitment and coordination. *Philos. Trans. R. Soc. B Biol. Sci.* **366**, 1554-1564.

Wakeling, J. M., Lee, S. S. M., Arnold, A. S., de Boef Miara, M. and Biewener, A. A. (2012). A muscle's force depends on the recruitment patterns of its fibers. *Ann. Biomed. Eng.* **40**, 1708-1720.

Ward, S. R., Eng, C. M., Smallwood, L. H. and Lieber, R. L. (2009). Are current measurements of lower extremity muscle architecture accurate? *Clin. Orthop. Relat. Res.* **467**, 1074-1082.

Winters, T. M., Takahashi, M., Lieber, R. L. and Ward, S. R. (2011). Whole muscle length-tension relationships are accurately modeled as scaled sarcomeres in rabbit hindlimb muscles. *J. Biomech.* **44**, 109-115.

Wolf, S. L., Ammerman, J. and Jann, B. (1998). Organization of responses in human lateral gastrocnemius muscle to specified body perturbations. *J. Electromyogr. Kinesiol.* **8**, 11-21.

Zajac, F. E. (1989). Muscle and tendon: properties, models, scaling, and application to biomechanics and motor control. *Crit. Rev. Biomed. Eng.* **17**, 359-411.

Table S1. Characteristics of the 16 cyclists tested.

Subject	Sex	Age (y)	Height (cm)	Body Mass (kg)	LG Max Isometric Force (N)*	MG Max Isometric Force (N)*	LG tendon Stiffness (N mm^{-1})†	MG tendon Stiffness (N mm^{-1})†
1	M	29	186	90.85	674	1179	34.5	63.2
2	M	28	167	68.00	588	1028	22.0	38.9
3	M	33	175	68.00	546	956	36.2	50.0
4	M	32	183	63.00	488	854	22.5	39.0
5	M	37	173	71.80	599	1047	39.2	55.0
6	M	30	179	70.30	555	972	24.5	41.8
7	M	47	183	86.50	661	1157	42.7	59.1
8	M	31	183	82.80	676	1184	26.3	41.2
9	F	30	167	65.80	584	1022	34.5	73.6
10	F	43	174	64.40	552	966	28.9	55.4
11	F	24	171	65.80	571	999	27.8	52.0
12	F	26	167	58.00	500	874	22.1	47.2
13	F	22	160	51.30	474	830	25.3	43.4
14	F	23	168	68.00	608	1065	29.5	58.8
15	F	20	165	67.30	622	1089	26.9	42.4
16	F	32	167	59.40	541	948	38.2	59.2

* Estimates of the muscles' maximum isometric force-generating capacity based on the muscles' volumes (Handsfield et al., 2014) and optimal fibre lengths (Arnold et al., 2010), assuming a maximum isometric muscle stress σ_0 of 225 kPa. (Spector et al., 1980; Roy et al., 1982).

†Linear region LG and MG AT stiffnesses were estimated as the proportion of the total AT stiffness contributed by each muscle based on ratio of the maximum force-generating capacity F_{max} of either the LG or MG to the combined triceps surae maximum force.

Table S2. Chi-square test results for comparison of r^2 and RMSE between one-element and two-element Hill-type muscle models.

Cadence (r.p.m.)	Load (N m)	Coefficient of determination, r^2		RMSE	
		two-element (% total)	*p*-value	two-element (% total)	*p*-value
60	44	46.9	0.73	37.5	0.15
80	14	59.4	0.29	28.1	0.01
80	26	62.5	0.16	43.8	0.47
80	35	65.6	0.07	43.8	0.47
80	44	59.4	0.29	46.9	0.72
100	26	71.9	**0.01***	62.5	0.15
120	13	68.8	**0.03***	68.8	**0.03***
140	13	71.9	**0.01***	68.8	**0.03***

Values in % total column indicate the number of times for the combined MG and LG results across individual subjects and pedalling conditions, as a %, that the two-element model performed better (higher r^2 and lower RMSE) (*n*=16). Differences were considered significant at the $p<0.05$ level.
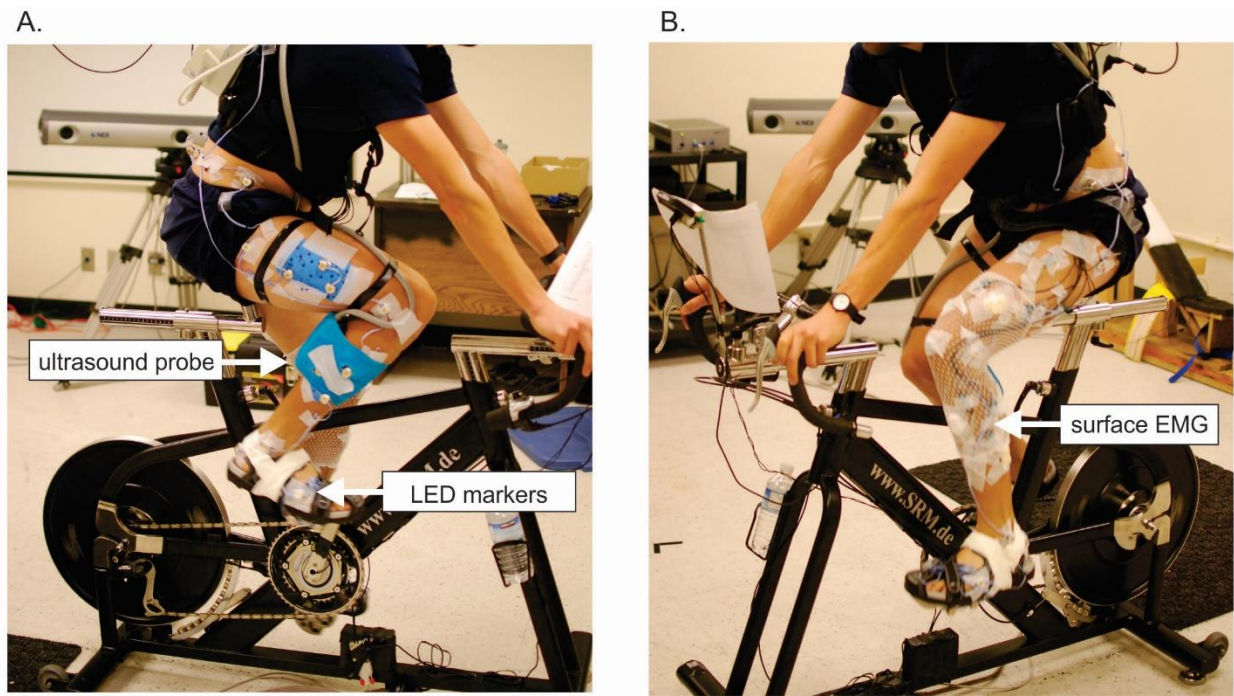*indicates $p<0.05$

Fig. S1. Experimental set up displaying B-mode ultrasound probe positioned over the LG muscle belly to image muscle fascicles and LED motion capture markers to record kinematics (A) and surface EMG electrodes placed on contralateral limb to record simultaneous muscle excitations (B).
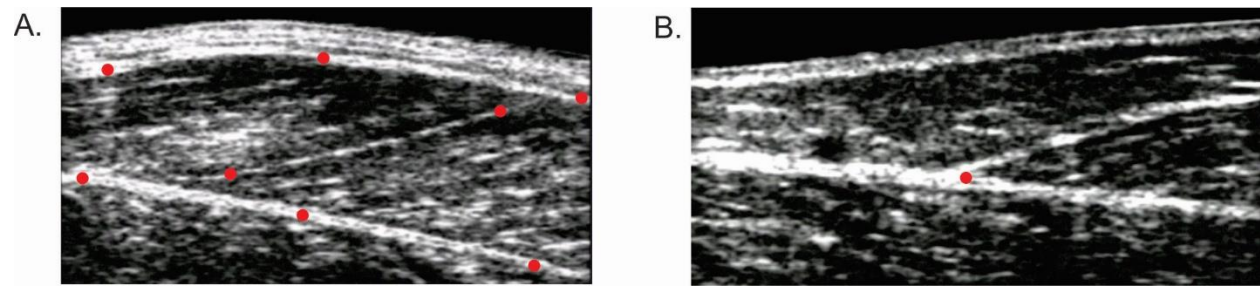
Fig. S2. B-mode ultrasound images of the MG muscle belly (A) and MG muscle-tendon junction (B). Red dots indicate digitized points that were used to determine time-varying fascicle lengths and pennation angles from (A) and tendon lengths from (B).
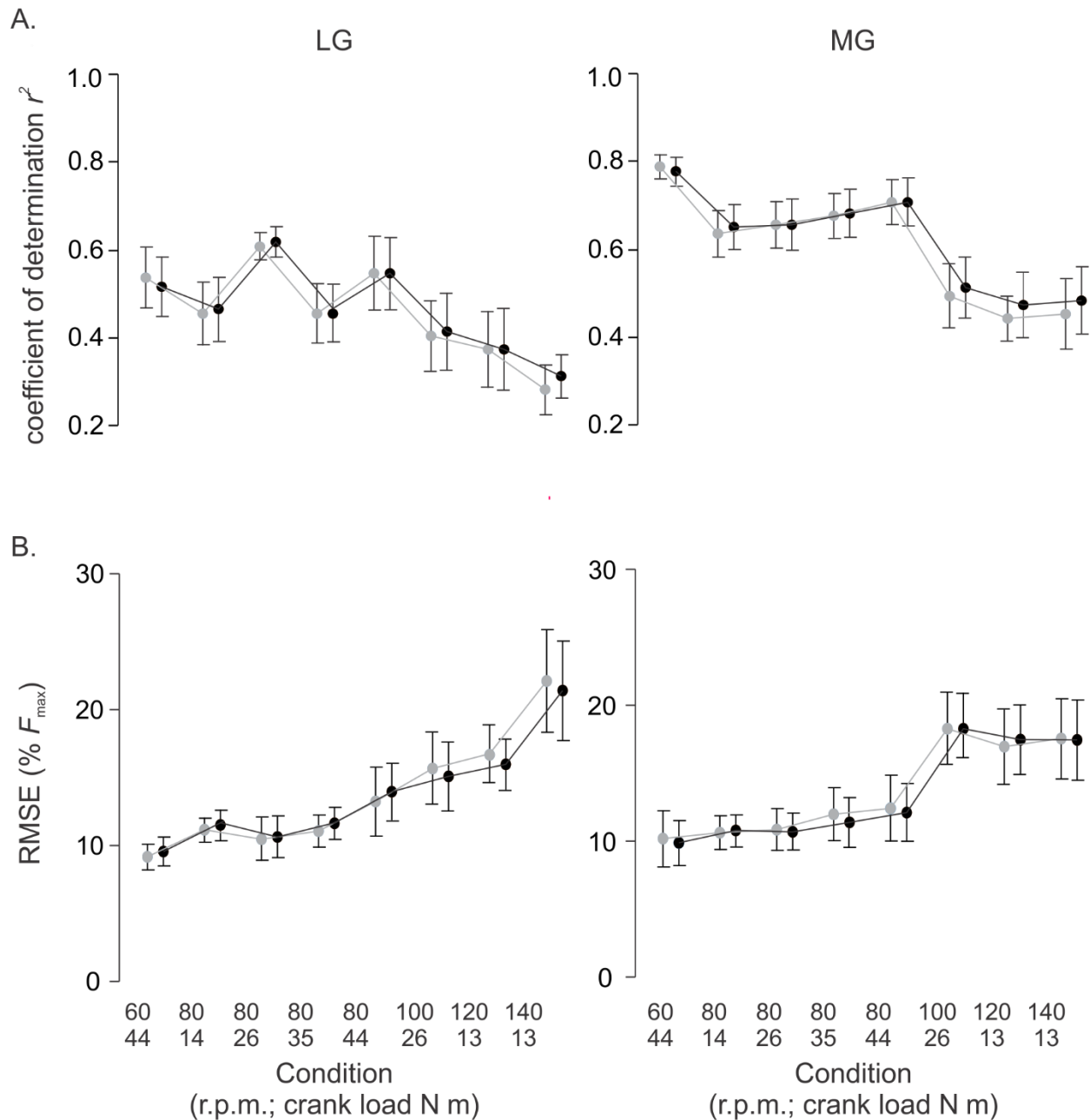
Fig. S3. Model predictions differ between muscles, pedalling conditions, and model type. Comparison of the one-element (grey) and two-element (black) Hill-type models using r^2 (A) and RMSE (B) across the pedal cycle for the LG and MG. Data points shown represent the mean ± SE across all subjects at each pedalling condition.